Digital image correlation and the use of high-speed cameras for 3D displacement monitoring in 1g small-scale landslide models

Nina Čeh[(1)], Josip Peranić[(1)], Vedran Jagodnik[(1)], Sara Pajalić[(1)], Martina Vivoda Prodan[(1)], Željko Arbanas[(1)]

1) University of Rijeka, Faculty of Civil Engineering, Rijeka, Radmile Matejčić 3, Croatia, +38551265956 (nina.ceh@uniri.hr)

Abstract Small-scale physical models of landslides triggered by rainfall and seismic conditions provide a good insight into the initiation and progression of full-scale landslides in nature. In order to track and document the displacements on the surface of the small-scale model, a digital image correlation-based optical measuring system with high-speed cameras is used here. Each model is prepared for the optical measurements by adding specially chosen marker points (pins) that are monitored by a pair of high-speed cameras during each experiment. An additional set of non-high-speed cameras with higher resolution is used to monitor the deformation field on a selected smaller part of the model. This enables to obtain the 3D displacements and velocities of each marker point in order to detect any movement or crack opening on the surface both visually and accurately from the optical measurement results. The described system and established measurement procedure are advantageous as they provide the 3D displacement and velocity data for a large number of points on the surface with less equipment than conventional contact measurement methods. The collected data, in combination with other monitoring sensors, allow the observation of landslide initiation and the analysis of landslide evolution in all parts of the model slope during the sliding process. In this paper we present the measurement procedure and the results obtained optically in selected small-scale experiments.

Keywords: landslides, 1g small-scale models, digital image correlation, optical measurement, surface displacements.

Introduction

Landslides are one of world's major hazards with serious consequences for both infrastructure and human lives. Heavy and prolonged rainfall alone and in combination with dynamic events such as earthquakes increase landslide risk (Petley 2012). Monitored and well-documented laboratory experiments conducted on small-scale landslide models allow a better understanding of the conditions that influence and trigger landslide initiation, as well as the investigation of possible landslide mitigation measures.

Motivated by this, a research project with an extensive experimental programme on small-scale landslide models was initiated (Arbanas et al 2019; 2020), with an aim to investigate the behaviour of structures used for mitigation of landslides triggered in static or dynamic conditions. Static conditions imply rainfall, whereas dynamic conditions imply earthquake excitation (in combination with significant saturation of the soil in a slope) (Pajalić et al. 2021).

In order to monitor the displacement field at the slope surface in a small-scale landslide model, it is necessary to use an approach that does not interfere with the model's geometry and the mass distribution on the slope. Non-contact optical measurement systems are chosen here, which can replace most of the conventional measurement devices for displacement and strain, as shown in Hunger and Morgenstern (1984), Okura et al. (2002), Moriwaki et al. (2004), Orense et al. (2004), Suits et al. (2009), Scaioni et al. (2013), Ooi et al. (2014), Lu et al. (2015) or Feng et al. (2016).

Digital image correlation (DIC) and optical measuring system

A 3D optical measuring system comprises a set of two cameras connected to a control unit and a suitable software used to conduct the measurement as well as post-process the data (Dobrilla et al. 2018; Čeh et al. 2018). Here we use two optical measuring systems: GOM Aramis 4M and GOM Aramis 12M. Their characteristics are given in Tab. 1.

The optical measuring procedure consists of calibration (with respect to the measuring volume or size of the monitored surface), surface preparation (which includes dyeing the whole surface or attaching marker points at discrete positions of interest, as shown in Fig. 1), measurement (obtaining pairs of snapshots at a given

Table 1 Characteristics of the two Aramis optical measuring systems.

System	Frame rate	Resolution (pixels)
Aramis 4M	168 fps	2400 × 1728
	1300 fps	2400 x 168
Aramis 12M	25 fps	4096 × 3000 pixels (full resolution)
	75 fps	4096 × 1000 pixels (1/3 of image)
	100 fps	Reduced resolution (binning)

Figure 1 Pins with attached markers on the surface of the model.

frequency throughout the experiment) and post-processing of the raw data. The results in the form of displacements of the surface points are obtained based on digital image correlation procedure in the post-processing, whereas the strains, velocities and any other values need to be derived from the displacements.

Experimental set-up (experiment on 14 February 2022)

The analysed experiment was conducted on a sandy slope with an angle of 35° exposed to a constant rainfall intensity of 73 mm/min (Arbanas et al. 2020; Pajalić et al. 2021b). The optical measuring equipment is positioned as shown in Fig. 2 for all experiments with static conditions: the high-speed Aramis 4M system positioned to capture the entire surface of the model, and the high-resolution 12M system focused on a small part on the side of the model.

The view from the left and right cameras of the 4M system is shown in Fig. 3, with the detected points marked in green. With a grid of 5 by 24 points, a total of 120 points were monitored. The experiment was optically monitored for 2 hours and 11 minutes, with a lower measurement frequency at the beginning, which was increased when surficial movements were detected (Tab. 2).

Results

The results are presented for the longitudinal profile shown in Fig. 4, which begins with point 2,1 in the lower part of the slope and ends with point 2,24 in the upper part of the slope. The position data of some markers are lost during the experiment due to water droplets accumulating on the markers and physical obstacles such as the elements of the sprinkler system or the reinforcements of the plexiglass side walls. Longitudinal profile 2 is chosen here for analysis, as all points (except point 2,1) were visible to both cameras. In addition to the profile considered, Fig. 4 shows the location of 2 points that are analysed in more detail due to their particular location in relation to the development of the landslide: points 2,19 and 2,21 near the upper part of the slope.

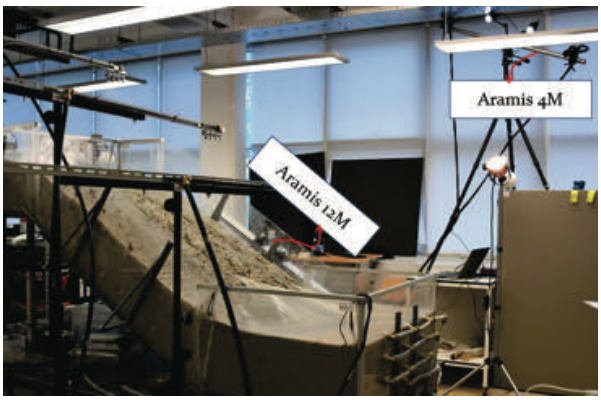

Figure 2 Setup of the optical measuring system in models subjected to static loading conditions (simulated rainfall).

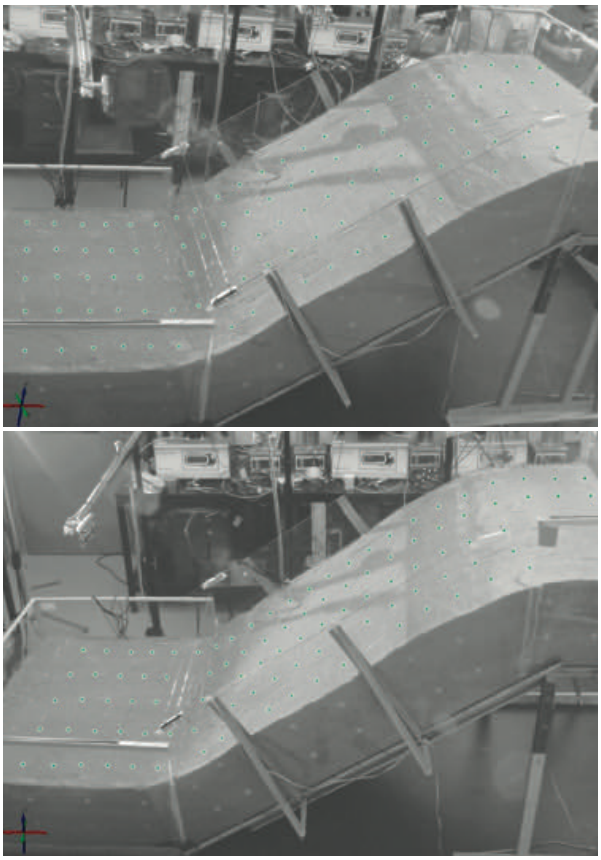

Figure 3 Left-camera (top) and right-camera (bottom) view of the model with monitored points (green dots) (from Maksimović (2020), Pajalić et al. (2021)).

Table 2 The measuring frequency and duration of the optical measuring system.

Part	Measuring frequency	dt	Duration
1	1/300 fps	300 s	52 min 59 s
2	1/10 fps	10 s	1 h 18 min 11 s

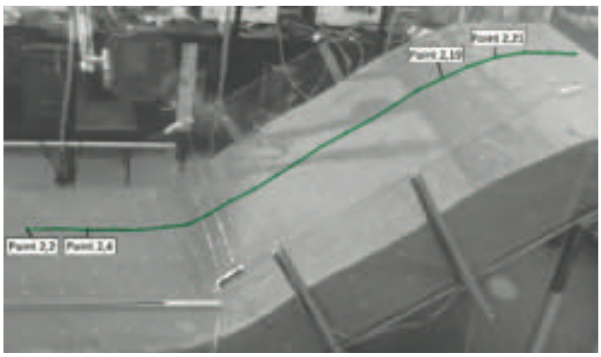

Figure 4 Longitudinal profile no. 2 in the reference stage and the location of the points used for the detailed analysis of the displacement evolution.

The orientation of the coordinate system used with the corresponding signs is given in Fig. 5. The shape of the profile throughout the experiment is shown in Fig. 6 (top). There is clear evidence of the development of larger displacements in the top of the slope between stages 300 and 434, specifically between stages 390 and 434. These stages correspond to a test time of 121 and 128 minutes (or 7262 and 7702 seconds) after the start of the test, i.e. the rainfall simulation (see Fig. 6, bottom). Snapshots of stages 390 and 434 from the left camera are also shown in Fig. 13.

The behaviour of the points in the upper part of the slope in profile 2 is analysed in detail. The points at the top were not covered by water at any time during the rainfall simulation, so, the both cameras were able to take clear photos of them until the end of the experiment. The time courses of the vertical displacements for the two chosen points (2,19 and 2,21) (marked in Fig. 4) are shown in Fig. 7.

Fig. 7 shows that the vertical displacements of the monitored points in the upper part of the slope are close to zero until about 3700 seconds (which roughly corresponds to the time when the first instability at the very bottom of the slope is noticed), which is followed by a slow linear increase until the last part of the experiment, when a rapid non-linear increase occurs, announcing a failure of the slope. This can also be seen in Fig. 8, where the stage (i.e. time) corresponding to the significant increase in displacements and cracking at the top of the slope can be accurately identified.

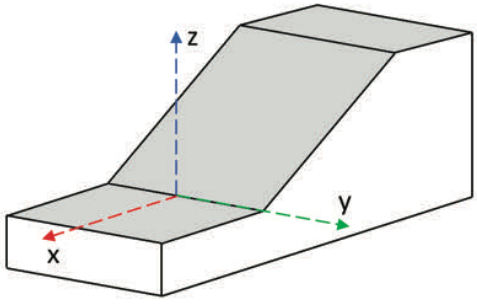

Figure 5 Coordinate system orientation used in the optical measurement and post-processing.

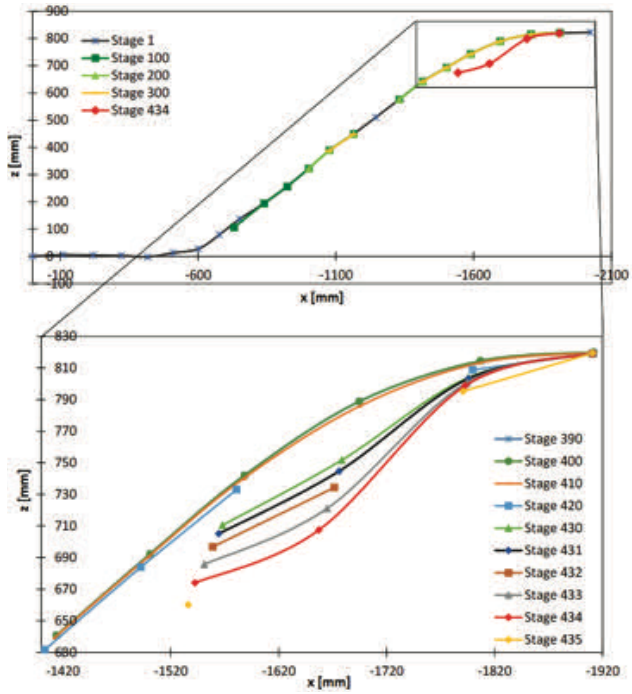

Figure 6 Longitudinal profile no. 2 shown in the x-y plane throughout the experiment (top) and the upper part of the profile between stage 390 and 435 (bottom) (Maksimović 2020; Pajalić et al. 2021).

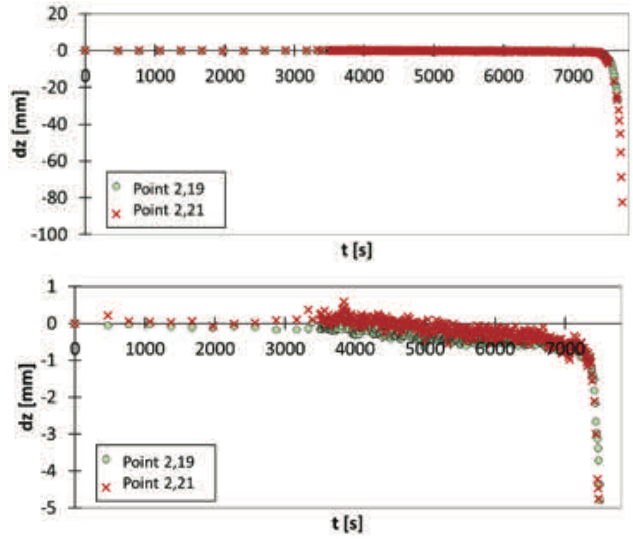

Figure 7 Time course of the displacements along the z-axis of points 2,19 and 2,21 in the upper part of the scaled slope: displacements on a scale up to -100 mm (top) and up to -5 mm (bottom).

A similar behaviour can be observed for the time courses of the horizontal displacements (Figs. 9 and 10). The two horizontal directions are defined so that the x-direction is longitudinal and the y-direction is transverse (see Fig. 5). Positive and negative values in the y-direction mean a movement down and up the slope, respectively, while positive and negative values in the x-direction mean a movement to the right and to the left, respectively, as seen from the crown.

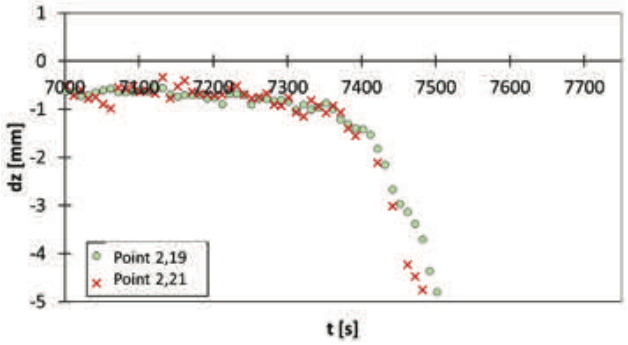

Figure 8 Time course of the displacements along the z-axis of points 2,19 and 2,21 between 116 and 130 minutes in the experiment (7000 and 7800 seconds, respectively).

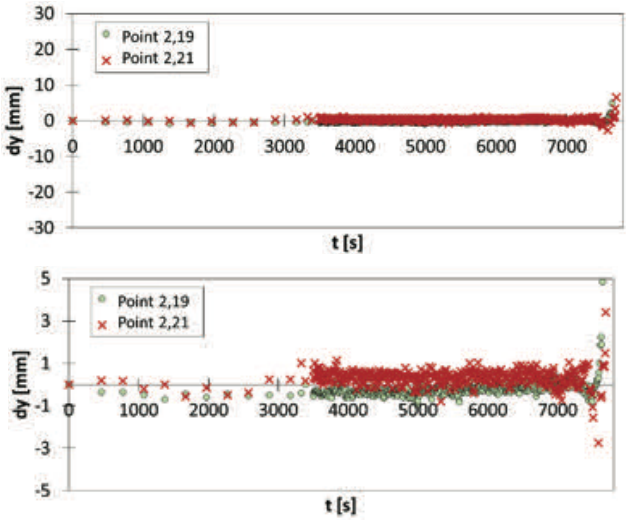

Figure 9 Time course of the displacements along the y-axis of points 2,19 and 2,21 in the upper part of the scaled slope: displacements on a scale up to -30 mm (top) and up to -5 mm (bottom).

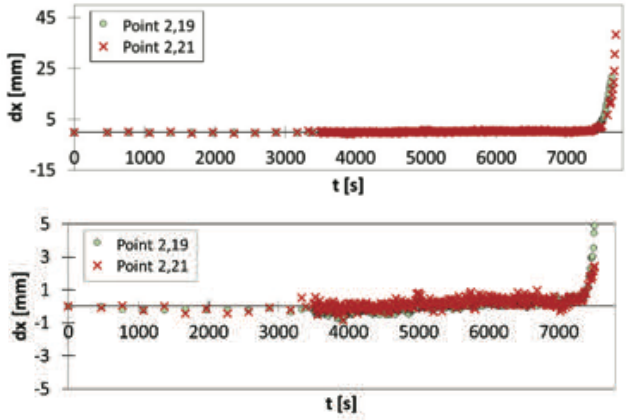

Figure 10 Time course of the displacements along the x-axis of points 2,19 and 2,21 in the upper part of the scaled slope: displacements on a scale from -15 to 45 mm (top) and from -5 to 5 mm (bottom).

We can again notice a slow linear increase between 3700 and 7500 seconds and a significant non-linear increase after that in x direction displacements, while y direction displacements increase as well, but the displacements are lower. Both directions are better analysed in Figs. 11 and 12, where the time when the displacements start to increase in a non-linear manner can be determined more precisely. A series of nine snapshots taken by the left camera during the last part of the experiment is shown in Fig. 13.

An increase in the vertical displacements of points 2,19 and 2,21 in Figs. 6-11 is presented after t=7400 s. However, as can be seen from stage 420 (t=7562 s) in Fig. 12, it is difficult to see only by visual inspection of the scaled slope model, that the points experience significant movements in the period before they are affected by the retrogressive sliding, as can be clearly seen for stage 430 (t=7662 s) in the same figure. The rapid increase in vertical displacements in Fig. 7 corresponds to the progression of instability in the form of the retrogressive sliding towards the top of the slope. As given in Tab. 2 the optical measurements are obtained from snapshots taken every 10 seconds in this part of the experiment, which results in 10 snapshots between the two stages of interest: stage 420 and 430. The used optical system, however, is able to monitor the model with frequency up to 168 fps, but limited to less than 60 seconds of continuous monitoring due to RAM capacity of the system. It is important to note that the time from the first instability in the model, which took a form of small rotational slide at the foot of the slope due to groundwater level rise, to when the retrogressive slide reached the analysed points at the top

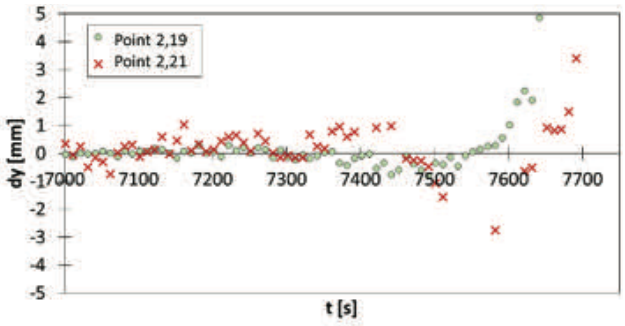

Figure 11 Time course of the displacements along the y-axis of points 2,19 and 2,21 in the upper part of the scaled slope.

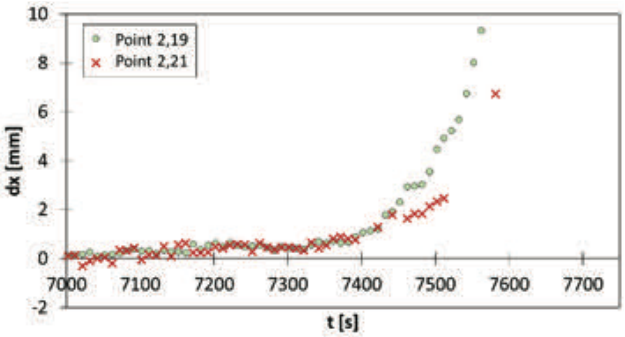

Figure 12 Time course of the displacements along the x-axis of points 2,19 and 2,21 in the upper part of the scaled slope. .

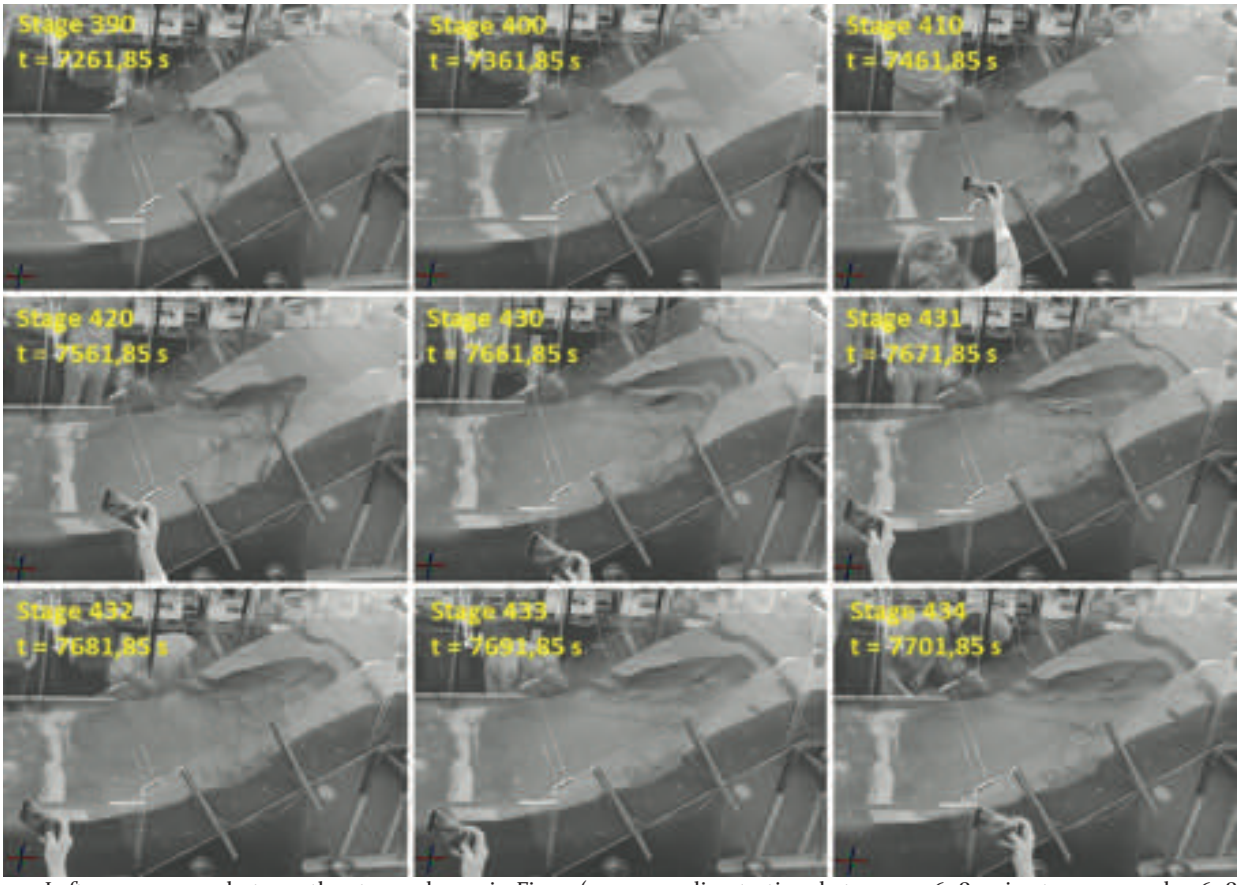

Figure 13 Left camera snapshots on the stages shown in Fig. 4 (corresponding to time between 7261.85 s in stage 390 and 7261.85 s in stage 434).

of the slope was about 60 minutes. Thus, monitoring the entire instability evolution with high frequency is not possible. These observations suggest that in a case where high frequency data of surface displacements are needed, i.e. in the analysis of processes that develop relatively quickly after a long period of inactivity, as is the case with fast moving flow-like landslides, rockfalls and tracking of the rockfall trajectories and/or the impact forces and interaction of fast moving slope material with the landslide remediation structures in scaled slope models etc., the usefulness of the non-contact measurement system, as the one presented in this study, becomes limited due to the requirement of postprocessing of the measurement data. However, the data obtained concurrently with some of the conventional landslide monitoring techniques (geodetic and geotechnical) that allow real-time monitoring of displacements or other quantities that can be used as indications that the scaled slope is approaching conditions of instability could be used to adjust the frequency of data collection and optimise the monitoring process of such non-contact systems during all phases of instability development, i.e. from stable conditions through the phase of initiation of movement, development and to deposition at the end. This could be the approach that would provide adequate data for a detailed analysis of the instability process and the mechanisms involved.

Discussion and Conclusions

Displacement data of the slope surface obtained with an optical measurement technique from the experiment conducted on a small-scale sandy slope initiated by simulated rainfall are presented. Two non-contact optical measurement systems, a high-speed camera system and a slower system with higher resolution, are used to monitor the 3D displacements of the surface of the model. Based on sets of snapshots from two precisely tuned cameras, the displacements of the marker points on the slope are obtained, post-processed and analysed.

One of longitudinal profiles of interest is presented here, where it is easy to keep a track of the profile shape throughout an experiment. Furthermore, the displacement data of two selected points at the top of the slope, combined with a series of snapshots, show how a significant increase in displacement can be detected and used to accurately detect any instability or cracking. Such an optical measurement method using high-speed camera systems in combination with other monitoring sensors installed in the model can provide much important and

well-documented data describing the behaviour of the surface in a small-scale landslide test.

This paper presented the results of a single test conducted to present the basic data that can be provided by this type of monitoring. The possibilities that the digital image correlation offers and the use of high-speed cameras for 3D displacement monitoring in small-scale landslide models are far greater and will be used in further analyses of landslide initiation and evolution in subsequent steps of the Project. The precision offered by this monitoring system will enable the following data that cannot be registered by the human eye: measurements of the deformation caused by the change in the unit weight of the soil and the stress changes during the infiltration of the rain; 3D displacements of the marker points on the slope surface, taking into account all the components of the displacement vectors; identification of the displacement rate in different parts of the slope and cross-relationships with data obtained from other monitoring sensors (tensiometers, accelerometers, MEMS, etc.). Analyses of these data will ensure significantly better insight into landslide initiation and evolution of landslides in small-scale landslide models as well as in real landslides on slopes made of similar soil materials.

Acknowledgments

This work is supported by Croatian Science Foundation under the Project IP-2018-01-1503 Physical modelling of landslide remediation constructions behaviour under static and seismic actions (ModLandRemSS).

References

Arbanas Ž, Jagodnik V, Peranić J, et al (2020) Physical Model of Rainfall Induced Landslide in Flume Test : Preliminary Results. Proceedings of 4th European Conference on Physical Modelling in Geotechnics - ECPMG 2020, 15-17 March 2020. Luleå, Sweden. pp. 115-122.

Arbanas Ž, Pajalić S, Jagodnik V, et al (2019) Development of physical model of landslide remedial constructions' behaviour. Proceedings of the 4th Regional Symposium on Landslides in the Adriatic - Balkan Region, 23-25 October 2019. Sarajevo, Bosnia and Herzegovina. pp 103–108

Čeh N, Jelenić G, Bićanić N (2018) Analysis of restitution in rocking of single rigid blocks. Acta Mechanica. 229:4623–4642. https://doi.org/10.1007/s00707-018-2246-8

Dobrilla S, Čeh N, Tuhtan M, Jelenić G (2018) Eksperimentalna analiza odziva grednog nosača na nejednoliku pobudu oslonacaExperimental Analysis of Structure Response to Non-uniform Support Excitation. Zbornik radova. 20:175–188. https://doi.org/10.32762/zr.20.1.11

Feng T, Mi H, Scaioni M, et al (2016) Measurement of Surface Changes in a Scaled-Down Landslide Model Using High-Speed Stereo Image Sequences. Photogrammetric Engineering & Remote Sensing. 82:547–557. https://doi.org/10.14358/PERS.82.7.547

Hunger O, Morgenstern NR (1984) Experiments on the flow behaviour of granular materials at high velocity in an open channel. Géotechnique. 34:405–413. https://doi.org/10.1680/geot.1984.34.3.405

Lu P, Wu H, Qiao G, et al (2015) Model test study on monitoring dynamic process of slope failure through spatial sensor network. Environmental Earth Sciences. 74:3315–3332. https://doi.org/10.1007/s12665-015-4369-8

Maksimović S (2020) Analiza površinskih pomaka na modelu klizišta. University of Rijeka, Faculty of Civil Engineering, Rijeka, Croatia. (in Croatian).

Moriwaki H, Inokuchi T, Hattanji T, et al (2004) Failure processes in a full-scale landslide experiment using a rainfall simulator. Landslides. 4:277–288. https://doi.org/10.1007/s10346-004-0034-0

Okura Y, Kitahara H, Ochiai H, et al (2002) Landslide fluidization process by flume experiments. Engineering Geology. 66:65–78. https://doi.org/10.1016/S0013-7952(02)00032-7

Ooi GL, Wang YH, Tan PS, et al (2014) An instrumented flume to characterize the initiation features of flow landslides. Geotechnical Testing Journal. 37(5). https://doi.org/10.1520/GTJ20130158

Orense R, Shimoma S, Maeda K, Towhata I (2004) Instrumented Model Slope Failure due to Water Seepage. Journal of Natural Disaster Science. 26:15–26. https://doi.org/10.2328/jnds.26.15

Pajalić S, Peranić J, Maksimović S, et al (2021) Monitoring and Data Analysis in Small-Scale Landslide Physical Model. Applied Sciences. 11:5040. https://doi.org/10.3390/app11115040

Petley D (2012) Global patterns of loss of life from landslides. Geology. 40:927–930. https://doi.org/10.1130/G33217.1

Scaioni M, Lu P, Feng T, et al (2013) Analysis of spatial sensor network observationsduring landslide simulation experiments. European Journal of Environmental and Civil Engineering. 17:802–825. https://doi.org/10.1080/19648189.2013.822427

Suits LD, Sheahan TC, Olivares L, et al (2009) An Instrumented Flume to Investigate the Mechanics of Rainfall-Induced Landslides in Unsaturated Granular Soils. Geotechnical Testing Journal. 32:101366. https://doi.org/10.1520/gtj101366